iScience

CellPress
OPEN ACCESS

Article

Terahertz waves regulate the mechanical unfolding of tau pre-mRNA hairpins

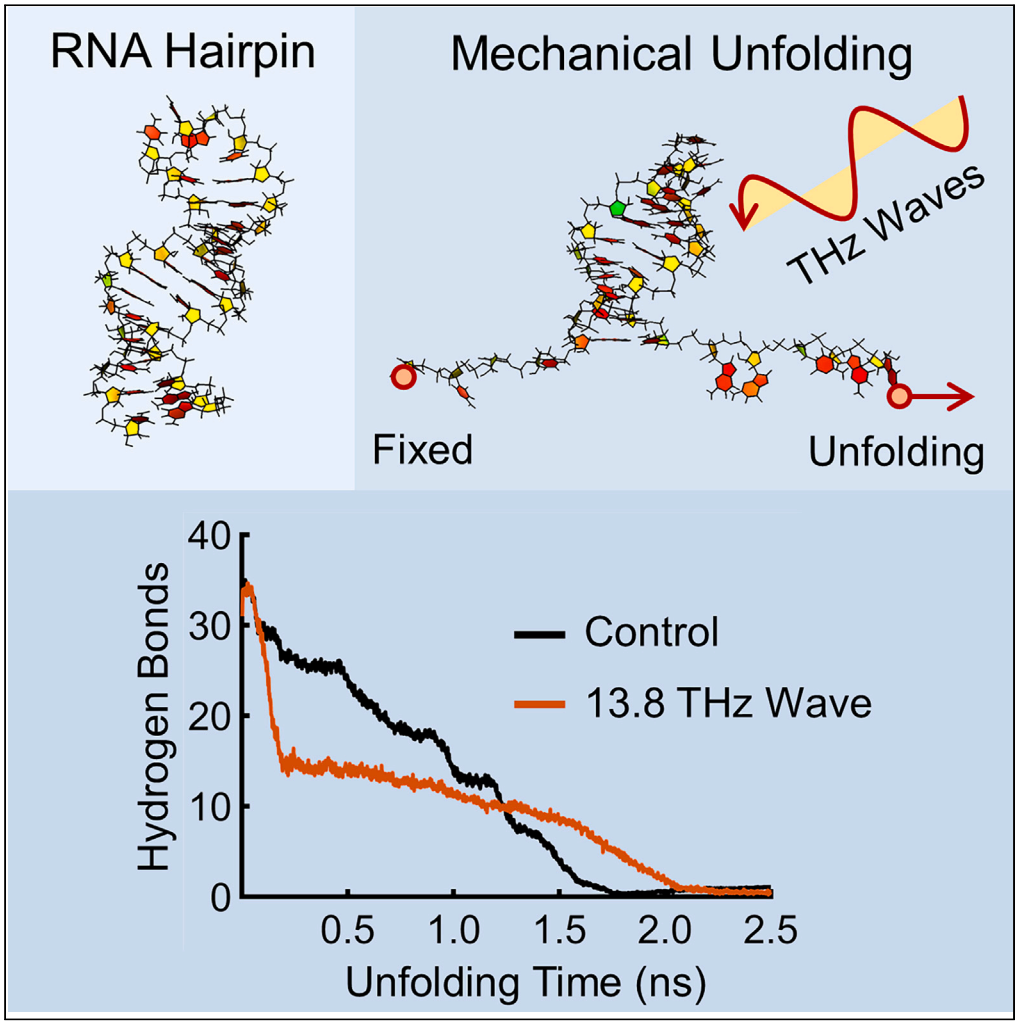

Qin Zhang, Lixia Yang, Kaicheng Wang, Lianghao Guo, Hui Ning, Shaomeng Wang, Yubin Gong

yanglixia@uestc.edu.cn (L.Y.)
ybgong@uestc.edu.cn (Y.G.)

Highlights

SMD unveiled THz wave influence on RNA stabilities and dynamics

0.1–41.2 THz waves regulate RNA unfolding via diverse mechanisms

The polarized direction of THz waves needs to be verified with statistical tests

Zhang et al., iScience 26, 107572
September 15, 2023
https://doi.org/10.1016/j.isci.2023.107572

iScience

CellPress
OPEN ACCESS

Article

Terahertz waves regulate the mechanical unfolding of tau pre-mRNA hairpins

Qin Zhang,[1] Lixia Yang,[2,*] Kaicheng Wang,[1] Lianghao Guo,[1] Hui Ning,[1] Shaomeng Wang,[1] and Yubin Gong[1,3,*]

SUMMARY

Intermolecular interactions, including hydrogen bonds, dominate the pairing and unpairing of nucleic acid chains in the transfer process of genetic information. The energy of THz waves just matches with the weak interactions, so THz waves may interact with biomolecules. Here, the dynamic effects of THz electromagnetic (EM) waves on the mechanical unfolding process of RNA hairpins (WT-30nt and its mutants, rHP, SARS-CoV-2, and SRV-1 SF206) are investigated using steered molecular dynamics (SMD) simulations. The results show that THz waves can either promote the unfolding of the double helix of the RNA hairpin during the initial unfolding phase (4–21.8 THz) or significantly enhance (23.8 and 25.5 THz) or weaken (37.4 and 41.2 THz) its structural stability during unfolding. Our findings have important implications for applying THz waves to regulate dynamic deconvolution processes, such as gene replication, transcription, and translation.

INTRODUCTION

Weak intermolecular interactions including hydrogen bonds and van der Waals forces, along with the collective vibrations of biomolecules (such as nucleic acids and proteins), as well as vibrational transitions of energy levels, occur within the THz band.[1] This band offers a theoretical basis for the interactions between biomolecules and THz waves. In recent years, considerable theoretical investigations and experimental confirmations have focused on the interactions between THz waves and nucleic acids, primarily concentrating on DNA molecules.[2–9]

Research in this area commences by exploring the frequencies of DNA vibrations and the patterns of stretching. THz radiation possesses the ability to resonate and excite low-frequency vibrational modes within the hydrogen bond network of water (2.4–6 THz) and the stretching mode of double-stranded DNA (6 THz).[2] At the microscopic level, THz wave may cause resonance excitation of DNA hydrogen bond, or even local fracture, and influence proton dynamics, thus resulting in alterations in gene expression,[3–5] while some of these studies use simplified models that ignore the factors of vibrational relaxation and solvation, and the theoretical calculation results differ from the actual situation.[10] In the macro effect, experimental and molecular dynamics (MD) simulation studies have shown that alternating electric fields of microwave and THz waves promote the unwinding rate of DNA under heating conditions.[6,8] Additionally, THz waves can impact the structure and yield of DNA self-assembly, whether the system is heated or at room temperature.[7,9] Nonetheless, RNA molecules participate in a broader array of biological processes compared to DNA, exhibiting a more flexible and unstable structure. Consequently, the mechanisms underlying the interaction between THz waves and RNA are likely to be more diverse and complex. Regrettably, only a limited number of relevant studies have elucidated the microscopic kinetic mechanisms involved in this context.

The structure-function relationships of biomacromolecules, such as hydrogen bonds that stabilize the secondary structures or electrostatic interactions between charged side chains, can also be studied by steered molecular dynamics (SMD). SMD is a derivative of MD simulation that imposes a directional force on a biomolecule to investigate the responses induced by external forces.[11] SMD simulations have been used to reduce the pathways and dynamic mechanisms of DNA, RNA, and RNA-protein biomacromolecules unfolding, such as the relationships between the mechanical unfolding process and the pull site of parallel G-quadruplex from human telomeric DNA,[12] the pathway of double-stranded RNA to single-stranded RNA molecules,[13] the unfolding behaviors of streptomycin-binding RNA aptamer under force,[14] the complexation and dissociation mechanism of small interfering RNA and PMAL carrier,[15] and the unfolding pathway of positive strand RNA turnip crinkle virus of T-shaped structure.[16] On the other hand, SMD simulation is also employed to study the stability of weak interactions between RNA and protein macromolecules, such as the minor-groove base triples formed in the mRNA pseudoknot improving the mechanical stability,[17] the additional interaction introduced by the N501Y mutation in the receptor-binding domain of spike protein strengthening the interactions between COVID-19 and its receptor ACE2,[18] and the stable base triple unfolding intermediate revealing importance in the pseudoknot-induced frameshift.[19]

In this paper, we conducted SMD theoretical simulations to study the interactions between THz waves and a pre-mRNA splice site hairpin of the microtubule-associated protein tau (MAPT). The alternative splicing of exon 10 determines the ratio of the MAPT repeat domain

[1]School of Electronic Science and Engineering, University of Electronic Science and Technology of China, Chengdu, Sichuan 611731, China
[2]School of Physics, University of Electronic Science and Technology of China, Chengdu, Sichuan 611731, China
[3]Lead contact
*Correspondence: yanglixia@uestc.edu.cn (L.Y.), ybgong@uestc.edu.cn (Y.G.)
https://doi.org/10.1016/j.isci.2023.107572

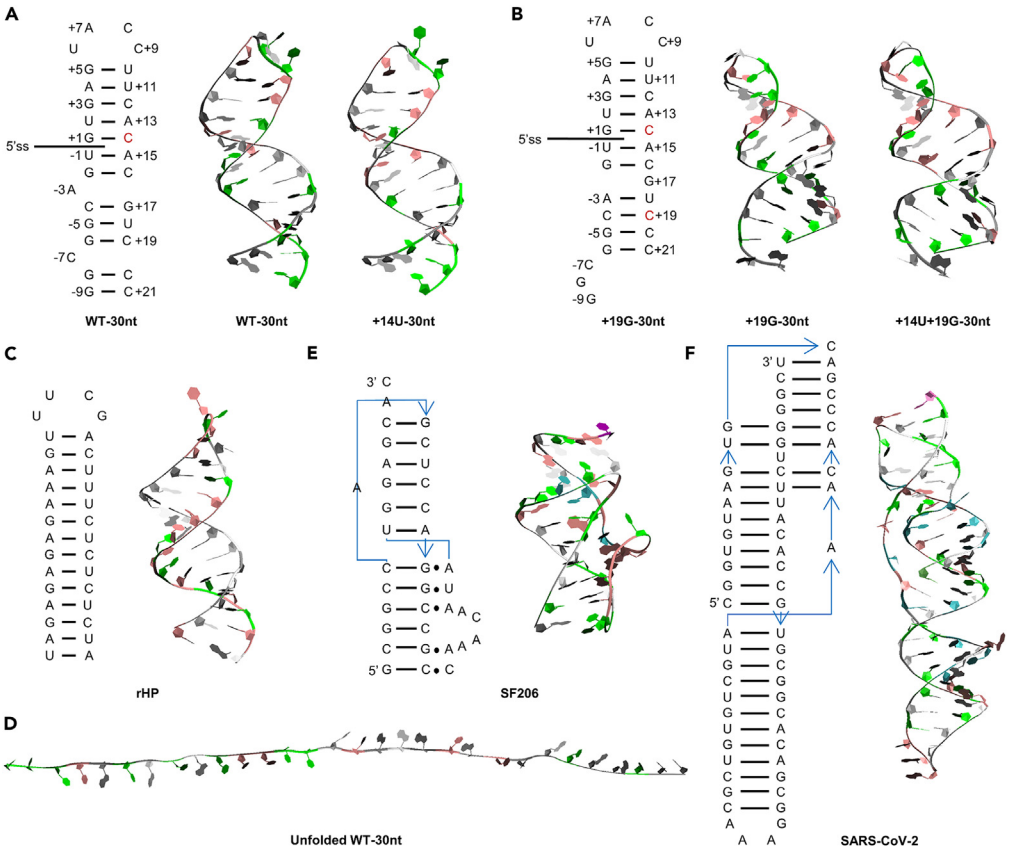

Figure 1. RNA 2D and 3D structures

3D structures obtained from the initial structures generated online by the Vfold3D tool after Gromacs energy minimization, with different colors drawn by base names (G, C, A, and U are shown in gray, green, white, and pink, respectively).

(A) The secondary structure of RNA WT-30nt and the tertiary structure of RNA WT-30nt and +14U used for simulation. The +14 nucleotide C labeled red is substituted with U in the mutation +14U.

(B) The secondary structure of RNA +19G-30nt and the tertiary structure of RNA +19G-30nt and +14U+19G-30nt used for simulation. The +14 nucleotide C and +19 nucleotide C labeled in red are substituted with U and G, respectively, in the mutation +14U+19G.

(C) The secondary structure and the tertiary structure of RNA rHP used for simulation.

(D) Unfolded WT-30nt formed by the unfolding of folded WT-30nt.

(E) The secondary structure and the tertiary structure of SF206 used for simulation.

(F) The secondary structure and the tertiary structure of SARS-CoV-2 used for the simulation.

(3R: 4R), while too high (or low) of this ratio (4R: 3R ratio remains about 1:1 in humans) has been associated with some neurodegenerative diseases such as Alzheimer's disease and dementia.[20,21] The alternative splicing of exon 10 is related to the stability of the regulatory hairpin at the splice site.[22,23] Here, our focus was to elucidate the impact and regulation of diverse THz wave properties, such as frequency, amplitude, and polarized direction, on the unfolding process of the regulatory hairpin (30 nucleotide wild-type, WT-30nt) and its mutants (+14U-30nt, +19G-30nt, +14U+19G-30nt), through extensive SMD simulations. Furthermore, we also verified whether the interaction rule of WT-30nt and its mutants with THz waves could be applied to other structures (32-mer RNA hairpin, rHP, SARS-CoV-2, and SRV-1 SF206). This work further provides theoretical support for the applications of THz waves in the regulations of DNA/RNA translation, DNA replication, translation, recombination, DNA repair, and other cellular metabolic processes involving nucleic acid chain separation.

RESULTS AND DISCUSSION

IR absorption spectra of folded WT-30nt and unfolded WT-30nt

Figure 1 shows the molecular structure of folded WT-30nt and unfolded WT-30nt RNAs. As seen in Figure 2, the absorption peaks of TIP3P water at 250–1000 cm^{-1} (7.5–30 THz) correspond well to the experimental results of ordinary water at 35°C,[24] while the peaks at 1500–1750 cm^{-1} (45–52.5 THz) and the higher peaks (82.5–112.5 THz) do not. This inconsistency may be due to adopting the TIP3P water molecule model and the single-precision version of Gromacs. We are interested in where the folded WT-30nt and unfolded WT-30nt spectra differ, as this may reflect changes in the absorption peaks introduced by the mechanical unfolding process (breaking of hydrogen bonds).

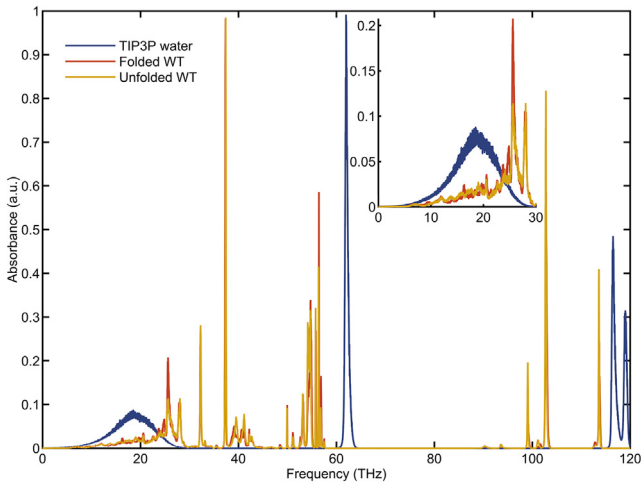

Figure 2. The IR absorption spectra of TIP3P water, folded WT-30nt, and unfolded WT-30nt in an aqueous solution
The absorbance is normalized. The small box in the upper right corner is the zoomed-in local spectral squares.

In Figure 2, the infrared (IR) curves between the folded WT-30nt and unfolded WT-30nt RNAs are significantly different. At lower frequencies (0–10 THz), the two curves show little difference, except for a redshift at 6.6 THz and a new absorption peak at about 9.5 THz for the folded WT-30nt. Between 10 and 20 THz, the two curves are quite different from each other, where 16.3 THz is a new absorption peak for the folded WT-30nt, at which they gradually increase absorbance. Between 20 and 40 THz, the folded WT-30nt possesses two unique peaks at 23.8 and 24.8 THz, and two minor red shifts at about 32.2 and 37.4 THz were observed. Higher frequency (between 42 and 120 THz) absorption peaks barely respond to the structural changes brought up by the unfolding of WT-30nt, so this frequency band is out of our discussion here.

THz waves regulate the mechanical unfolding process of WT-30nt RNA hairpins

We employed Vfold3D online tools to predict and produce 3D structures in our RNA mechanical unfolding study.[25–27] In this section, we are going to discuss the effect of the frequency, amplitude, and polarized direction of THz electromagnetic (EM) waves on the mechanical unfolding process of WT-30nt. In the first part, we only discuss the mechanical unfolding process of WT-30nt with pull force along the y direction and without the THz waves (see Video S1). Figure S1 illustrates the linear relation between simulated time and extended length, which shows the pulling type is constant velocity pull. Many peaks and valleys in Figure S2 may imply the paired hydrogen bonds are starting to break. We combine Figures S2 and S3 to uncover how the WT-30nt unfolds. The arrows in Figure S2 correspond to the breaking of the first base pair, the second, …, and the twelfth base pair, respectively, which shows our pull parameters (force constant and pull rate) are reasonable to reflect the mechanical unfolding process of WT-30nt RNA and other similar structures. Three pulling modes were used in experiment,[20] in which the critical force of the constant-force mode of WT-30nt was 13.5 pN, while the mean pull force of the SMD simulation was about 332 pN (200 kJ/mol/nm), which presents many times different. According to a previous similar paper,[17] our SMD simulation of the pulling rate (10 nm/ns) was faster. Still, the tested unfolding speed of 1 nm/ns could not clearly reflect the unfolding progress from the time-force curves for our RNA system. Previous papers reported these differences.[17,28] So, the simulation results here can only be a qualitative comparison.

In the second part, based on IR absorption spectra in Figure 2, we selected 24 (0.1–41.2 THz) frequencies to systematically investigate the impact of THz wave frequencies on the RNA mechanical unfolding. Surprisingly, distinct ranges of THz waves exhibit varying effects on the RNA unfolding, demonstrating clear frequency selectivity. Notably, in Figure 3, EM waves with frequencies ranging from 0.1 to 2 THz exerted negligible influence on the RNA unfolding process compared to cases without THz waves (noE). This observation suggests that the interaction between EM waves within the 0.1–2 THz and WT-30nt is insufficient to impact the unfolding process significantly. However, during the 1.2 ns unfolding stage of WT-30nt under the influence of a 3 THz wave, the overall pull force intensifies, signifying the initiation of interaction between the THz wave and WT-30nt.

As shown in Figure 4, applying 4–21.8 THz waves significantly increases the force to unfold WT-30nt (compared to noE and 23.8–41.2 THz). As shown in Figures 5 and S5, the binding energy and number of hydrogen bonds during RNA unfolding decrease sharply with increasing frequency in a shorter time when the EM wave frequency is between 4 and 13.8 THz. By checking the unfolding trajectory of WT-30nt under EM waves between 4 and 13.8 THz, after a particular simulation time, we discover that the double-strand WT-30nt unspins, opens hydrogen bonds, and falls along the unfolding direction to form a structure with more complex interactions, thus requiring a more significant force to unfold (see Video S2). However, 13.8 THz is a turning frequency, and when the EM wave frequency is between 16.3 and 21.8 THz, the decrease in binding energy and the number of the hydrogen bond is moderated with increasing frequency, and the unfolding trajectory of WT-30nt is similar to the above (4–13.8 THz).

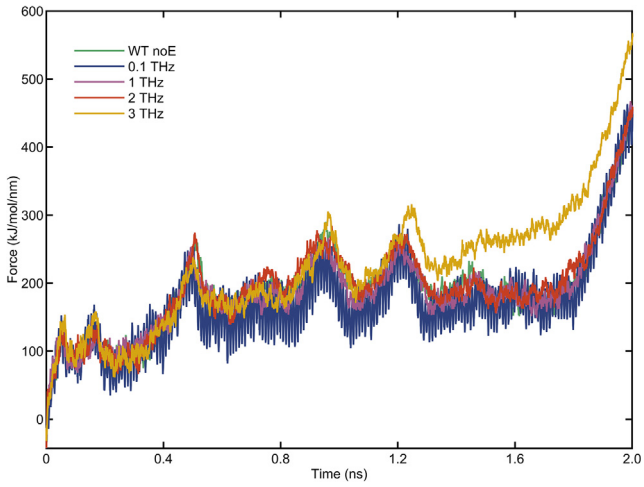

Figure 3. The curves of pulling force and unfolding time of WT-30nt with 0.1–3 THz, 0.5 V/nm, y-polarized EM waves

All noE in this paper is the control group and represents without THz waves. An average of 20 sets plots all curves of the pulling force.

According to existing literature, the absorption features of nucleic acid molecules in the submillimeter-wave range (2–300 cm^{-1}, 0.006–9 THz) are associated with the weak bonds and non-bonded interactions (van der Waals forces, dispersion forces, and hydrogen bonding) of the molecule, and the internal motions of base pair weak hydrogen bonds, helical twisting, and bending, as low-frequency vibrations, are sensitive to the length, configuration, and topological structure of nucleic acid molecules.[29–31] In contrast, the vibration pattern of nucleic acids at 9–15 THz (300–500 cm^{-1}) is related to the ribose ring vibrations.[30] The impact of 4–21.8 THz waves on the unfolding process of WT-30nt is remarkably different. On one hand, this could be attributed to the enhancement of weak interactions between base pairs or the amplification of ribose ring vibrations, leading to duplex unwinding and rapid hydrogen bond disruption during the dynamic unfolding process of WT-30nt. On the other hand, it is also related to the interaction between water molecules and THz waves. However, based on the results from Table S5 and Figure S4, we can exclude the influence of thermal effects caused by the strong absorption of THz waves by water molecules. The specific impact of 4–21.8 THz waves on the mechanical unfolding of WT-30nt indicates a frequency-selective influence (or modulation) of WT-30nt mechanical unfolding in the solution.

The pulling force or normalized energy required for WT-30nt unfolding decreases sequentially with 23.8–41.2 THz waves (except for 28.1 THz, see Figure 6). Figure 6 and Table 1 show no significant effect of THz waves on the binding energy of structurally stable folded WT-30nt. But a considerable effect on the unfolding process of WT-30nt indicates that the non-thermal biological effect of THz waves may have few impacts on the dynamics process of structural stability but an effect on the dynamic change. In Table 2, Figure 2, and Video S3, it can be seen that 23.8 THz is the frequency with the maximum energy required for unfolding WT-30nt, and it is also an absorption peak of the folded WT-30nt. The absorption characteristics of nucleic acids at 22.5–45 THz (750–1500 cm^{-1}) are related to the backbone vibration of phosphate

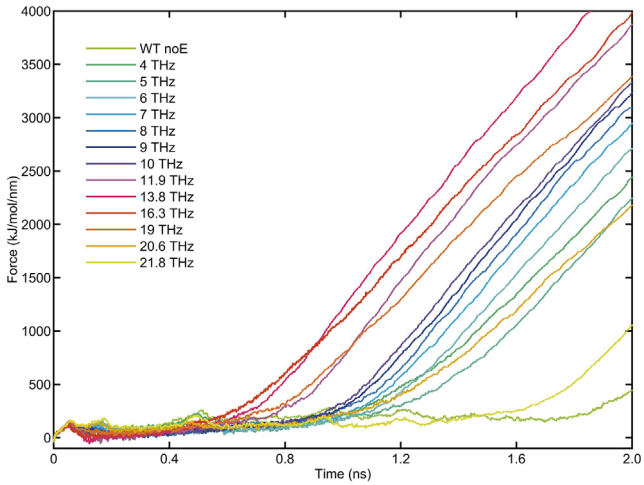

Figure 4. The curves of the pulling force and unfolding time of WT-30nt with 4–21.8 THz, 0.5 V/nm, y-polarized EM waves

An average of 20 sets plots the curves of the pulling force.

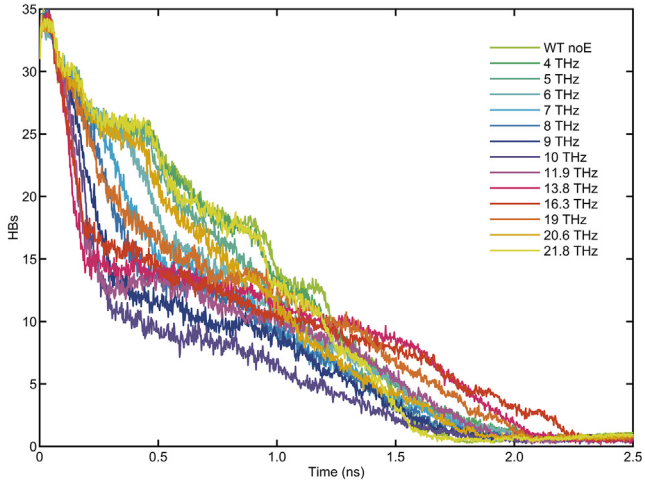

Figure 5. Changes in the total number of formed hydrogen bonds (HBs) among base pairs of WT-30nt with 4–21.8 THz, 0.5 V/nm, y-polarized EM waves
The WT-30nt structure (Figure 1A) is divided into two symmetric groups (-9G to +7A and +8C to +21C) to analyze the number of hydrogen bonds (30°, within 3.5 Å) between these two groups during mechanical unfolding. An average of 20 sets plots all the curves of HBs.

and are independent of the base sequence.[30] Therefore, this may be the key frequency for enhancing the stability of the sugar-phosphate backbone. We turned our attention to the last two frequencies, 37.4 and 41.2 THz, and found that they both made the WT-30nt unfold with less force compared to noE and THz waves at other frequencies, with 41.2 THz waves reducing the pulling force more and more significantly.

The third part investigates the effect of the amplitude of the THz waves on the mechanical unfolding of the WT-30nt. Figures 7, S6, and S7 show the linear impact of THz wave amplitude on the WT-30nt unfolding. For all frequencies except 10 THz, the pull force increases correspondingly with the enhancement of THz wave amplitude, making a more significant force required for WT-30 unfolding. The THz waves of 0.5 and 1 V/nm increased the average temperature during the unfolding process of the WT-30nt by up to 3 and 11.3 K (23.8 THz, in Table S5), respectively. The previously described analysis suggests that the 0.5 V/nm, 23.8–29.4 THz band is suitable for subsequent studies of the effects of THz waves on WT-30nt mutants and other structures.

In the fourth part, we explore the phenomenon of interference by different polarized directions of THz waves on the WT-30nt mechanical unfolding. Since the x- and z-polarized directions of EM waves are perpendicular to the y-polarized (also the pulling) direction, only the x- and y-polarized THz waves were investigated here to see if they have different effects on the WT-30nt mechanical unfolding. As shown in Table S2, the relative energy of unfolding WT-30nt by x-polarized EM waves at 23.8, 25.5, and 29.4 THz has a significant change compared to the same frequency in the y-polarized direction, which indicates that THz waves with different polarization directions have different significant effects on WT-30nt unfolding process. As seen in Figures 8 and S8, the tension curve of WT-30nt unfolding with 9, 10, and 11.9 THz x-polarized EM waves have a vast difference compared to the same frequency in y-polarized direction, which implies that the polarization direction of certain frequency THz waves may modulate the way or trajectory of WT-30nt unfolding. We examine the unfolding trajectory of the WT-30nt with the x-polarized EM wave at 9, 10, and 11.9 THz and find that the x-polarized THz wave causes the WT-30nt as a whole to remain relatively stationary at first in a direction perpendicular to the unfolding direction (y direction). The pull end unfolds hard along the y direction (11.9 THz is much easier than 9 and 10 THz). However, this is entirely different from how the y-polarized THz wave of the same frequency unfolds at the beginning (see the second part of this section).

Accordingly, we can also speculate that the polarization direction of the 4–21.8 THz wave significantly affects or changes the unfolding trajectory compared to the 23.8–29.4 THz band, thus affecting the pulling force to unfold the WT-30nt. According to the previously described analysis, the way of initial mechanical unfolding of WT-30nt is severely regulated by the polarization direction of some THz waves (this phenomenon differs from existing studies[32,33]), and there are also cases where the way is not regulated, which indicates that whether the polarized direction of THz waves affects the MD simulation has to be finally determined by combining the explored system, the EM frequency, the simulation method, and the study content. In summary, the polarization direction of THz waves may have little effect on some systems that are large, stable, and minor conformational changes in the MD process but may have an influence on some dynamic processes with directionality (e.g., ion channels), conformational changes, etc.

THz waves regulate the mechanical unfolding process of WT-30nt mutants

The +14U-30nt is the +14C to +14U mutation of WT-30nt. While, the +19G and +14U+19G adopted a structural rearrangement as reported before (Figure 1).[20] First, we studied the unfolding process of the WT-30nt mutants without the THz wave. As seen in Figure 9, the force required for RNA unfolding is about the same for each mutant, and it is difficult to determine the small and large visually. We found two spikes

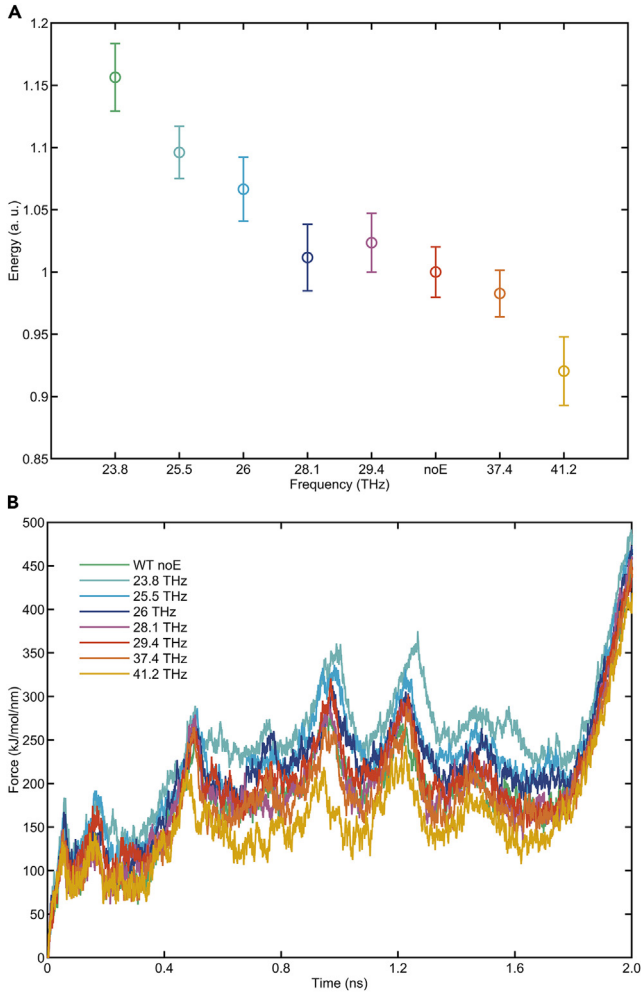

Figure 6. The effect of 23.8–41.2 THz, 0.5 V/nm, y-polarized EM waves on the WT-30nt mechanical unfolding

(A) Normalized energy of the mechanical unfolding process of WT-30nt under the action of THz waves. The dots in the vertical bar of noE are the average of 20 sets, set to 1, and the length of the vertical bar is the standard deviation range of 20 sets.

(B) The curves of pulling force and unfolding time of WT-30nt with THz waves. An average of 20 sets plots the curves of the pulling force.

for +14U (around 50 and 100 ps), which are due to the interaction between the four bases (no such problem was found for WT-30) of +14U when unfolding the first two base pairs (-9G-+21C and -8G-+20C), making the force needed to unfold these two base pairs very high fully. Therefore, we only compare the total pull force (relative energy) of +14U and WT-30nt between the complete break of the hydrogen bond of the 2nd base pair and the entire break (unfolding) of the hydrogen bond of the 12th base pair. As shown in Table S3, the relative energy of unfolding +14U is less than that of WT-30nt, indicating that WT-30nt is more stable than +14U, which is consistent with the previous experiment.[20] As for the stability of +14U+19G, +19G, and WT-30nt, we compared them by the relative energies (summation of the pull force in 2.5 ns time) between the start of their simulations and the complete unfolding of the hydrogen bond between the last base pair. As shown in Table S3, +14U+19G is the largest, while +19G and WT are about the same, a phenomenon that slightly differs from the previous experiment.[20] This is because we unfolded each mutant 20 times to take the average, while the previous investigation unfolded hundreds of times to take the average. In the force-ramp mode of the experiment, the loading force of WT and +19G had an overlap region, indicating that the forces of unfolding WT and +19G are comparable. So, it is reasonable to produce these differences described previously. In Table 2, the significance tests of each mutant relative to its relative energy without EM waves show that 23.8, 25.5, and 26 THz significantly increase the pull force and also make the structure more stable.

THz waves regulate the mechanical unfolding process of rHP, SARS-CoV-2, and SF206

The rHP hairpin, comprised of 32 nucleotides (nt), exhibits a loop-stem hairpin structure similar to WT-30nt but with two additional nucleotides and distinct sequences. The frameshifting pseudoknot RNA of SARS-CoV-2 consists of 66 nt and contains a single pseudoknot motif, whose

Table 1. The impact of THz waves on folded WT-30nt

Amp (V/nm)	Fre (THz)	μ (kJ/mol)	σ (kJ/mol)	*t*
0.5	4	−1424.1	20.4783	–
	10	−1420.0	28.4295	–
	23.8	−1423.7	23.7463	–
	25.5	−1422.3	32.5754	–
	26.0	−1416.2	24.6331	–
	28.1	−1422.3	24.3538	–
	29.4	−1422.3	33.5263	–
	37.4	−1412.2	27.0621	–
	41.2	−1416.1	25.0445	–
noE		−1417.9	32.2669	

μ, σ, and *t* are mean, root-mean-square error, and *t*-distribution test, respectively. There is no significant difference (denoted by the symbol "–", <90%) in the binding energy at all the above THz frequencies compared to noE. See Table S1 for more details.

stability is intricately linked to frameshifting—a phenomenon intimately associated with viral infectivity.[34] Likewise, SF206, comprising 36 nt, exhibits base triples, with its stability also correlated with frameshifting.[17] To further investigate, we aim to ascertain whether the mechanical unfolding process of these three RNAs (rHP, SARS-CoV-2, and SF206) under the influence of 23.8–29.4 THz waves exhibits a similar or consistent pattern compared to WT-30nt and its mutants. As depicted in Figure 9, the unfolding curve of rHP closely resembles that of +14U+19G. Complementing the findings in Table 2, we ascertain that the intervention of 23.8 and 25.5 THz waves has a substantial impact on the mechanical unfolding of rHP, resulting in increased unfolding force. While there are variations in the unfolding parameters, the unfolding trajectory of SF206 (in Figures 9 and S10) aligns with previously reported findings.[17] Given the larger size of SARS-CoV-2 with 66 nt, both its unfolding time and that of the water box are increased, while the other parameters remain consistent with other unfolding entities. The unfolding trajectory of SARS-CoV-2 is illustrated in Figure S9.

In summary, our findings demonstrate that the intervention of 23.8 and 25.5 THz waves has the most pronounced impact on the mechanical unfolding of all studied RNA hairpins (WT-30nt, +14U, +19G, +14U+19G, rHP, SARS-CoV-2, and SF206). Based on our earlier analysis, these two EM frequencies are most likely related to specific patterns of covalent bonding and backbone vibrations inherent in nucleic acid molecules. These characteristics remain independent of the base pair sequence,[30,35,36] suggesting a significant influence on the structural stabilities of diverse RNAs, including hairpins, pseudoknots, or RNA structures containing base triples with arbitrary nucleotide sequences and lengths. Contrary to the conventional notion that all small biological molecules possess inherent vibrational frequencies, our observations reveal a universal THz frequency that remarkably enhances the required force for the mechanical unfolding of diverse RNA hairpins, thereby promoting their structural stability. This discovery serves as a crucial inspiration and provides a broader perspective for further exploration of the mechanisms underlying the biological effects of EM waves.

Table 2. The relative energy of the mechanical unfolding of all RNAs and the significance test

Fre (THz)	WT-30nt (μ/*t*)	+14U (μ/*t*)	+19G (μ/*t*)	+14U+19G (μ/*t*)	rHP (μ/*t*)	SF206 (μ/*t*)	SARS (μ/*t*)
noE	4.2586	5.5345	4.5330	4.7305	3.9757	4.2645	8.0334
23.8	4.9247 ***	6.1867 ***	5.2227 ***	5.4545 ***	4.6658 ***	4.9290 ***	11.171 ***
25.5	4.6678 ***	5.9321 ***	5.0049 ***	5.1466 ***	4.4460 ***	4.6743 ***	10.083 ***
26	4.5419 ***	5.8385 ***	4.8595 ***	5.0585 ***	4.3333 /	4.3628 /	9.6152 ***
28.1	4.3083 /	5.5918 /	4.6874 ***	4.8362 **	4.0160 /	4.2095 /	8.4123 ***
29.4	4.3589 **	5.6249 **	4.6646 **	4.7469 /	4.0336 /	4.2737 /	8.5814 ***

In Table 2, Fre (THz) represents the frequency of THz waves. The relative energy of each THz frequency was summed by the pulling force (except for SARS, the others are 2.5 ns) of an average of 20 sets. The index of 10^8 was ignored for each relative energy. The "*" represents the test of the significance of relative energy between a specific THz frequency and noE. *, **, and *** represent the significance levels of 0.05, 0.01, and 0.001 (pairwise *t* tests), respectively. See Table S4 for more details.

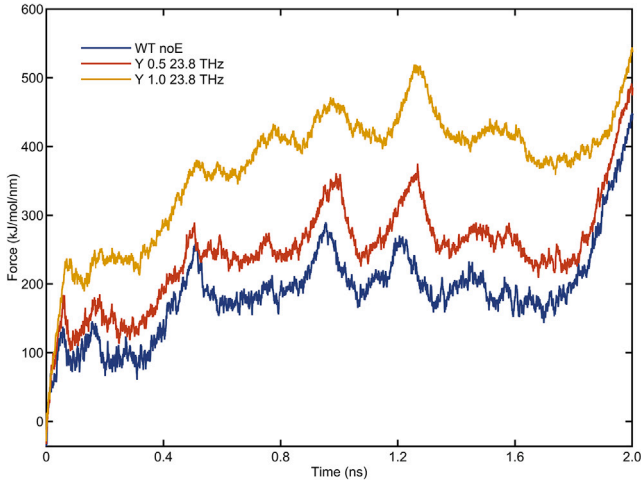

Figure 7. The curves of pulling force and unfolding time of WT-30nt with 23.8 THz, 0.5 and 1.0 V/nm, y-polarized EM waves

An average of 20 sets plots the curves of the pulling force. See Figures S6 and S7 for more comparisons.

Conclusion

In short, SMD simulations manifest that THz waves can intervene in the dynamic mechanical unfolding of RNA hairpins (WT-30nt and its mutants, rHP, SARS-CoV-2, and SF206). Specifically, 0.1–2 THz waves have little effect on the pulling force of the WT-30nt mechanical unfolding. The 0.5 V/nm and y-polarized THz waves at 4–21.8 THz promote the WT-30nt double helix to open hydrogen bonds in a particular time and to fall along the y-direction forming a more complex structure of interactions making the unfolding force increase abnormally. 37.4 and 41.2 THz waves significantly reduce the pulling force required for the mechanical unfolding of WT-30nt. The universal 23.8 and 25.5 THz, 0.5 V/nm, y-polarized EM waves significantly enhanced the structural stability of the unfolding processes of RNAs (arbitrary length and sequence or structures containing hairpin, pseudoknot, and base triple), which may be related to the THz waves enhancing the vibrational intensity of covalent bonds and backbone sugar during RNA mechanical unfolding. Compared to the y-polarized EM waves at 23.8, 25.5, and 29.4 THz, the impact of x-polarized THz waves on the unfolding process of WT-30nt is significantly different. This indicates that the polarization direction of THz waves needs to be taken into account during MD simulations. The polarization direction of EM waves at 9, 10, and 11.9 THz significantly affects the trajectories of WT-30nt unfolding in the initial stages. In contrast, 26 and 28.1 THz effects on the WT-30nt unfolding process are independent of the polarization direction. MD simulations showed that THz waves have no significant impact on the binding energy of the stable folded WT-30nt. In contrast, SMD simulations showed that THz waves significantly modulate the manner of dynamic mechanical unfolding of WT-30nt and the required pulling force for unfolding, suggesting that the non-thermal biological effects of THz waves may be achieved by influencing dynamic changing processes dominated by hydrogen bonds. According to the previously described analysis, THz

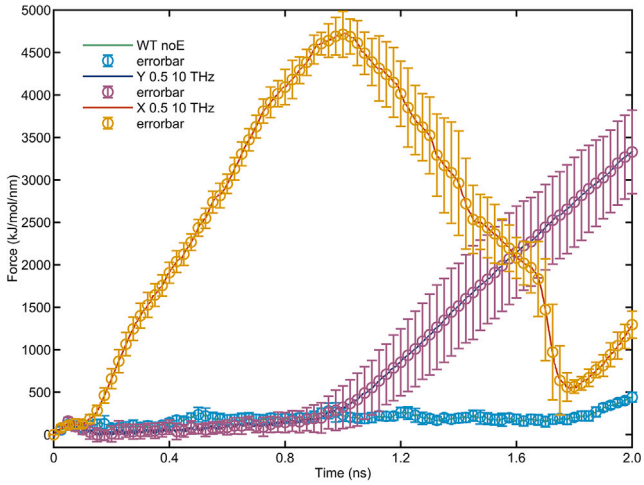

Figure 8. The curves of pulling force and unfolding time of WT-30nt with 10 THz, 0.5 V/nm, x- and y-polarized EM wave

An average of 20 sets plots the curves of the pulling force. Any errorbar is the deviation of the pulling force of 20 sets from the average pulling force, which takes one standard deviation. See Figure S8 for more comparisons.

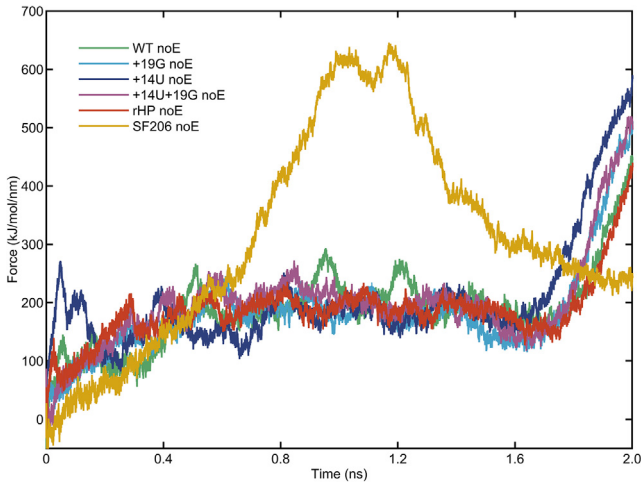

Figure 9. The curves of pulling force and unfolding time of RNAs pulled along the y direction

An average of 20 sets plots the curves of the pulling force. Total SMD time is 2.5 ns. We take a 2 ns (already fully unfolded) data plot.

waves in specific frequency bands can intervene in the chain unfolding process prevalent in biological processes such as gene transcription and translation by simulated helicases. Therefore, at least from the results of MD simulations, THz waves may regulate the dynamic chain separation processes, such as transcription, replication, and translation processes of genes, and may further affect gene expression and thus treat related diseases, such as Alzheimer's disease.

Limitations of the study

This paper has some limitations; we applied SMD to study the mechanical unfolding process of hairpin RNAs with the intervention of THz waves. We used the NVT ensemble during the SMD processes, and the pressures of the system varied considerably under 4–21.8 THz waves (this variation was also present in the NPT ensemble, more strongly). It is unknown whether this change in pressure affects the hairpin RNA unfolding process. Secondly, this paper simulates the mechanical unfolding process of hairpin RNAs in the solution environment, which can better reflect the process of unfolding RNA hairpin by single-molecule optical tweezers, but this is still different from the strand separation process mediated by helicase (such as pre-mRNA splicing and RNA transcription, which are more complex and diverse) that exists in biological metabolic processes. More experimental studies and theoretical validations are needed to further reveal the laws in this paper.

STAR★METHODS

Detailed methods are provided in the online version of this paper and include the following:

- KEY RESOURCES TABLE
- RESOURCE AVAILABILITY
  - Lead contact
  - Materials availability
  - Data and code availability
- EXPERIMENTAL MODEL AND SUBJECT DETAILS
- METHOD DETAILS
  - IR absorption spectra of folded and unfolded WT-30nt RNA
  - SMD simulations of RNA hairpins
  - MD simulations of folded WT-30nt RNA
- QUANTIFICATION AND STATISTICAL ANALYSIS

SUPPLEMENTAL INFORMATION

Supplemental information can be found online at https://doi.org/10.1016/j.isci.2023.107572.

ACKNOWLEDGMENTS

This work is supported by the National Natural Science Foundation of China (Grant Nos. T2241002, 32000914, 61921002, and 61988102).

AUTHOR CONTRIBUTIONS

Conceptualization, Q.Z. and L.X.Y.; Methodology, Q.Z. and L.X.Y.; Software, Q.Z. and K.C.W.; Formal Analysis, Q.Z. and K.C.W.; Resources, H.N. and L.H.G.; Writing – Original Draft, Q.Z.; Writing – Review & Editing, Q.Z., K.C.W., L.X.Y., and S.M.W.; Supervision, Y.B.G.

DECLARATION OF INTERESTS

The authors declare no competing interests.

INCLUSION AND DIVERSITY

We support inclusive, diverse, and equitable conduct of research.

Received: March 15, 2023
Revised: July 14, 2023
Accepted: August 5, 2023
Published: August 9, 2023

REFERENCES

1. Baxter, J.B., and Guglietta, G.W. (2011). Terahertz spectroscopy. Analytical chemistry *83*, 4342–4368.
2. Zhuang, W., Feng, Y., and Prohofsky, E. (1990). Self-consistent calculation of localized DNA vibrational properties at a double-helix–single-strand junction with anharmonic potential. Phys. Rev. *41*, 7033.
3. Chitanvis, S.M. (2006). Can low-power electromagnetic radiation disrupt hydrogen bonds in dsDNA? J. Polym. Sci. B Polym. Phys. *44*, 2740–2747.
4. Alexandrov, B.S., Gelev, V., Bishop, A.R., Usheva, A., and Rasmussen, K.Ø. (2010). DNA breathing dynamics in the presence of a terahertz field. Phys. Lett. *374*, 1214–1217.
5. Aleksandr, B. (2012). Interaction of terahertz radiation with DNA. Nanosystems: Physics, Chemistry, Mathematics *3*, 51–55.
6. Wu, K., Qi, C., Zhu, Z., Wang, C., Song, B., and Chang, C. (2020). Terahertz wave accelerates DNA unwinding: A molecular dynamics simulation study. J. Phys. Chem. Lett. *11*, 7002–7008.
7. Greschner, A.A., Ropagnol, X., Kort, M., Zuberi, N., Perreault, J., Razzari, L., Ozaki, T., and Gauthier, M.A. (2019). Room-temperature and selective triggering of supramolecular DNA assembly/disassembly by nonionizing radiation. J. Am. Chem. Soc. *141*, 3456–3469.
8. Sensale, S., Peng, Z., and Chang, H.-C. (2018). Acceleration of DNA melting kinetics using alternating electric fields. The Journal of chemical physics *149*, 085102.
9. Zhang, C., Yuan, Y., Wu, K., Wang, Y., Zhu, S., Shi, J., Wang, L., Li, Q., Zuo, X., Fan, C., et al. (2022). Driving DNA Origami Assembly with a Terahertz Wave. Nano Lett. *22*, 468–475. https://doi.org/10.1021/acs.nanolett.1c04369.
10. Markelz, A.G., and Mittleman, D.M. (2022). Perspective on Terahertz Applications in Bioscience and Biotechnology. ACS Photonics *9*, 1117–1126. https://doi.org/10.1021/acsphotonics.2c00228.
11. Do, P.-C., Lee, E.H., and Le, L. (2018). Steered molecular dynamics simulation in rational drug design. J. Chem. Inf. Model. *58*, 1473–1482.
12. Li, H., Cao, E.-h., and Gisler, T. (2009). Force-induced unfolding of human telomeric G-quadruplex: a steered molecular dynamics simulation study. Biochem. Biophys. Res. Commun. *379*, 70–75.
13. Mishra, R.K., Mukherjee, S., and Bhattacharyya, D. (2021). Maturation of siRNA by strand separation: Steered molecular dynamics study. J. Biomol. Struct. Dyn. *40*, 13682–13692.
14. Baptista, L.A., and Netz, P.A. (2019). Single molecule force spectroscopy of a streptomycin-binding RNA aptamer: An out-of-equilibrium molecular dynamics study. J. Chem. Phys. *151*, 195102.
15. Lu, Y., Li, J., and Lu, D. (2017). The mechanism for the complexation and dissociation between siRNA and PMAL: A molecular dynamics simulation study based on a coarse-grained model. Mol. Simulat. *43*, 1385–1393.
16. Kasprzak, W.K., Kim, T., Le, M.-T., Gao, F., Young, M.Y., Yuan, X., Seog, J., Simon, A.E., and Shapiro, B.A. (2018). Simulations of Optical Tweezers Experiments Reveal Details of RNA Structure Unfolding. Biophys. J. *114*, 214a–215a.
17. Zhong, Z., Yang, L., Zhang, H., Shi, J., Vandana, J.J., Lam, D.T.U.H., Olsthoorn, R.C., Lu, L., and Chen, G. (2016). Mechanical unfolding kinetics of the SRV-1 gag-pro mRNA pseudoknot: possible implications for– 1 ribosomal frameshifting stimulation. Sci. Rep. *6*, 1–14.
18. Tian, F., Tong, B., Sun, L., Shi, S., Zheng, B., Wang, Z., Dong, X., and Zheng, P. (2021). N501Y mutation of spike protein in SARS-CoV-2 strengthens its binding to receptor ACE2. Elife *10*, e69091.
19. Chang, K.-C., Hsieh, P.-S., Lee, A.-Y., Salawu, E., Lin, Y.-H., Chen, Y.-T., and Wen, J.-D. (2018). Unfolding Intermediate of mRNA Pseudoknot Correlates with Ribosomal Frameshifting. Biophys. J. *114*, 592a–593a.
20. Tan, J.Z., Yang, L.X., Ong, A.A.L., Shi, J.H., Zhong, Z.S., Lye, M.L., Liu, S.Y., Lisowiec-Wachnicka, J., Kierzek, R., Roca, X., and Chen, G. (2019). A Disease-Causing Intronic Point Mutation C19G Alters Tau Exon 10 Splicing via RNA Secondary Structure Rearrangement. Biochemistry *58*, 1565–1578. https://doi.org/10.1021/acs.biochem.9b00001.
21. Young, J.J., Lavakumar, M., Tampi, D., Balachandran, S., and Tampi, R.R. (2018). Frontotemporal dementia: latest evidence and clinical implications. Therapeutic Advances in Psychopharmacology *8*, 33–48. https://doi.org/10.1177/2045125317739818.
22. Donahue, C.P., Muratore, C., Wu, J.Y., Kosik, K.S., and Wolfe, M.S. (2006). Stabilization of the tau exon 10 stem loop alters pre-mRNA splicing. J. Biol. Chem. *281*, 23302–23306.
23. Buratti, E., and Baralle, F.E. (2004). Influence of RNA secondary structure on the pre-mRNA splicing process. Molecular and cellular biology *24*, 10505–10514.
24. Maréchal, Y. (2011). The molecular structure of liquid water delivered by absorption spectroscopy in the whole IR region completed with thermodynamics data. J. Mol. Struct. *1004*, 146–155. https://doi.org/10.1016/j.molstruc.2011.07.054.
25. Cao, S., and Chen, S.J. (2011). Physics-Based De Novo Prediction of RNA 3D Structures. J. Phys. Chem. B *115*, 4216–4226. https://doi.org/10.1021/jp112059y.
26. Xu, X., Zhao, P., and Chen, S.-J. (2014). Vfold: A Web Server for RNA Structure and Folding Thermodynamics Prediction. PLoS One *9*, e107504. https://doi.org/10.1371/journal.pone.0107504.
27. Humphrey, W., Dalke, A., and Schulten, K. (1996). VMD: Visual molecular dynamics. J. Mol. Graph. *14*, 33–38. https://doi.org/10.1016/0263-7855(96)00018-5.
28. White, K.H., Orzechowski, M., Fourmy, D., and Visscher, K. (2011). Mechanical unfolding of the beet western yellow virus– 1 frameshift signal. J. Am. Chem. Soc. *133*, 9775–9782.
29. Duong, T.H., and Zakrzewska, K. (1997). Calculation and analysis of low frequency normal modes for DNA. J. Comput. Chem. *18*, 796–811. https://doi.org/10.1002/(sici)1096-987x(19970430)18:6<796::Aid-jcc5>3.3.Co;2-g.
30. Globus, T.R., Woolard, D.L., Samuels, A.C., Gelmont, B.L., Hesler, J., Crowe, T.W., and Bykhovskaia, M. (2002). Submillimeter-wave Fourier transform spectroscopy of biological macromolecules. J. Appl. Phys. *91*, 6105–6113. https://doi.org/10.1063/1.1466878.
31. Globus, T., Bykhovskaia, M., Woolard, D., and Gelmont, B. (2003). Sub-millimetre wave absorption spectra of artificial RNA molecules. Journal of Physics D-Applied Physics *36*, 1314–1322. Pii s0022-3727(03)54121-3. https://doi.org/10.1088/0022-3727/36/11/312.

32. Li, Y., Chang, C., Zhu, Z., Sun, L., and Fan, C. (2021). Terahertz Wave Enhances Permeability of the Voltage-Gated Calcium Channel. J. Am. Chem. Soc. *143*, 4311–4318. https://doi.org/10.1021/jacs.0c09401.
33. Zhu, Z., Chang, C., Shu, Y., and Song, B. (2019). Transition to a superpermeation phase of confined water induced by a terahertz electromagnetic wave. J. Phys. Chem. Lett. *11*, 256–262.
34. Jones, C.P., and Ferré-D'Amaré, A.R. (2022). Crystal structure of the severe acute respiratory syndrome coronavirus 2 (SARS-CoV-2) frameshifting pseudoknot. RNA *28*, 239–249.
35. Bykhovskaia, M., Gelmont, B., Globus, T., Woolard, D.L., Samuels, A.C., Duong, T.H., and Zakrzewska, K. (2001). Prediction of DNA far-IR absorption spectra based on normal mode analysis. Theor. Chem. Acc. *106*, 22–27.
36. Sarkar, M., Dornberger, U., Rozners, E., Fritzsche, H., Strömberg, R., and Gräslund, A. (1997). FTIR Spectroscopic Studies of Oligonucleotides That Model a Triple-Helical Domain in Self-Splicing Group I Introns. Biochemistry *36*, 15463–15471. https://doi.org/10.1021/bi9702243.
37. Zgarbová, M., Šponer, J., Otyepka, M., Cheatham, T.E., III, Galindo-Murillo, R., and Jurečka, P. (2015). Refinement of the Sugar–Phosphate Backbone Torsion Beta for AMBER Force Fields Improves the Description of Z- and B-DNA. J. Chem. Theor. Comput. *11*, 5723–5736. https://doi.org/10.1021/acs.jctc.5b00716.
38. Zgarbová, M., Otyepka, M., Šponer, J., Mládek, A., Banáš, P., Cheatham, T.E., III, and Jurečka, P. (2011). Refinement of the Cornell et al. Nucleic Acids Force Field Based on Reference Quantum Chemical Calculations of Glycosidic Torsion Profiles. J. Chem. Theor. Comput. *7*, 2886–2902. https://doi.org/10.1021/ct200162x.
39. Van Der Spoel, D., Lindahl, E., Hess, B., Groenhof, G., Mark, A.E., and Berendsen, H.J. (2005). GROMACS: fast, flexible, and free. J. Comput. Chem. *26*, 1701–1718.
40. Martínez-González, J.A., Nandi, P.K., English, N.J., and Gowen, A.A. (2020). Infrared spectra and density of states at the interface between water and protein: Insights from classical molecular dynamics. Chem. Phys. Lett. *757*, 137867. https://doi.org/10.1016/j.cplett.2020.137867.
41. Du, J., Yao, N., Ma, X., Wang, H., Li, Q., and Feng, Z. (2023). Infrared spectra of the SARS-CoV-2 spike receptor-binding domain: Molecular dynamics simulations. Chem. Phys. Lett. *810*, 140176. https://doi.org/10.1016/j.cplett.2022.140176.
42. Henschel, H., Andersson, A.T., Jespers, W., Mehdi Ghahremanpour, M., and van der Spoel, D. (2020). Theoretical Infrared Spectra: Quantitative Similarity Measures and Force Fields. J. Chem. Theor. Comput. *16*, 3307–3315. https://doi.org/10.1021/acs.jctc.0c00126.
43. Agarwal, V., Huber, G.W., Conner, W.C., Jr., and Auerbach, S.M. (2011). Simulating infrared spectra and hydrogen bonding in cellulose Iβ at elevated temperatures. J. Chem. Phys. *135*, 134506. https://doi.org/10.1063/1.3646306.
44. Jorgensen, W.L., Chandrasekhar, J., Madura, J.D., Impey, R.W., and Klein, M.L. (1983). Comparison of simple potential functions for simulating liquid water. The Journal of chemical physics *79*, 926–935.
45. Bussi, G., Donadio, D., and Parrinello, M. (2007). Canonical sampling through velocity rescaling. The Journal of chemical physics *126*, 014101.
46. Berendsen, H.J., Postma, J.v., Van Gunsteren, W.F., DiNola, A., and Haak, J.R. (1984). Molecular dynamics with coupling to an external bath. The Journal of chemical physics *81*, 3684–3690.
47. Parrinello, M., and Rahman, A. (1980). Crystal structure and pair potentials: A molecular-dynamics study. Phys. Rev. Lett. *45*, 1196–1199. https://doi.org/10.1103/PhysRevLett.45.1196.
48. Parrinello, M., and Rahman, A. (1981). Polymorphic transitions in single crystals: A new molecular dynamics method. J. Appl. Phys. *52*, 7182–7190. https://doi.org/10.1063/1.328693.
49. Thomas, M., Brehm, M., Fligg, R., Vöhringer, P., and Kirchner, B. (2013). Computing vibrational spectra from ab initio molecular dynamics. Phys. Chem. Chem. Phys. *15*, 6608–6622.
50. Bo, W., Guo, L., Yang, Y., Ma, J., Wang, K., Tang, J., Wu, Z., Zeng, B., and Gong, Y. (2020). Numerical Study of Voltage-Gated Ca2+ Transport Irradiated by Terahertz Electromagnetic Wave. IEEE Access *8*, 10305–10315. https://doi.org/10.1109/ACCESS.2020.2964780.
51. Bergues-Pupo, A.E., Arias-Gonzalez, J.R., Morón, M.C., Fiasconaro, A., and Falo, F. (2015). Role of the central cations in the mechanical unfolding of DNA and RNA G-quadruplexes. Nucleic acids research *43*, 7638–7647.

STAR★METHODS

KEY RESOURCES TABLE

REAGENT or RESOURCE	SOURCE	IDENTIFIER
Software and algorithms		
Gromacs version 2020.03	Van Der Spoel et al.[39]	https://www.gromacs.org/
Vfold3D 2.0	Cao and Chen[25] Xu et al.[26]	http://rna.physics.missouri.edu/vfold3D2/
VMD version 1.9.3	Humphrey et al.[27]	https://www.ks.uiuc.edu/Research/vmd/

RESOURCE AVAILABILITY

Lead contact

Further information and requests for resources should be directed to the Lead Contact, Yubin Gong (ybgong@uestc.edu.cn).

Materials availability

This study did not generate new unique reagents.

Data and code availability

- All data reported in this paper will be shared by the lead contact upon request.
- This paper does not report original code.
- Any additional information required to reanalyze the data reported in this paper is available from the lead contact upon request.

EXPERIMENTAL MODEL AND SUBJECT DETAILS

Our study does not use experimental models typical in the life sciences.

METHOD DETAILS

IR absorption spectra of folded and unfolded WT-30nt RNA

The single precision version of Gromacs 2020.3 and the amber14sb OL15 force field plus χOL3 RNA patch,[37–39] parametrization of the glycosidic torsion χ, were employed to calculate the IR absorption spectra of the WT-30nt RNA. We also cite some cases of calculating IR spectra of biomolecules with MD.[40–43] In pre-equilibrium, we chose the flexible TIP3P water,[44] the best collocation of the amber14sb force field, and confined the heavy atoms. Then, we employed the V-rescale temperature coupling (300 K)[45] and Berendsen pressure coupling (1 bar).[46] In production MD, firstly, we chose the flexible TIP3P water, changed the Berendsen pressure coupling to Parrinello-Rahman,[47,48] and removed all constraints involving covalent bonds. Then the system was simulated for 1 ns to total relaxation. Next, based on the already relaxed structures, we only changed the time step to 1 fs and saved the compressed coordinates every 4 fs, and simulation for 100 ps, which process was performed 500 times for folded and unfolded WT-30nt RNA. Subsequently, we extracted the dipole moment data from the MD trajectory. The dipole moment data were then processed by using the autocorrelation function and Fourier transform according to the following formula to obtain IR intensity[49]

$$A(\omega) \propto \int \langle \dot{\mu}(\tau)\dot{\mu}(t+\tau)\rangle_{\tau} e^{-i\omega t} dt \qquad \text{(Equation 1)}$$

where $\dot{\mu}(\tau)$ is the time derivative of the dipole vector. In the end, we got the THz absorption spectra of the folded and unfolded WT-30nt RNA, and 50 ns in principle plotted each spectrum.

SMD simulations of RNA hairpins

We selected the amber14sb OL15 force field plus χOL3 RNA patch for SMD simulations.

First, we will discuss how to simulate THz EM waves in MD. We know from some simulation cases that when EM waves interact with charged particles, their magnetic field component is several orders of magnitude smaller than the electric field component, and the electric field plays

a dominant role.[32,50] Therefore, the electric fields were used to represent THz waves during the simulation with Gromacs in this paper. The general expression for the THz electric field is given by:

$$E(t) = E_0 \exp\left[-\frac{(t - t_0)^2}{2\sigma^2}\right]\cos[\omega(t - t_0)] \quad \text{(Equation 2)}$$

Where E_0, σ, ω, t_0 are electric field amplitude, pulse width, pulse angular frequency, and pulse maximum time point, respectively. All MD simulations in this paper apply a THz sinusoidal electric field.

In pre-equilibrium, we chose the rigid water and constrained all covalent bonds. Then, we employed the V-rescale temperature coupling (295 K) and Berendsen pressure coupling (1 bar). In SMD simulations, at the very beginning, we chose the isothermal-isobaric ensemble (V-rescale tau_t 0.2 ps and Parrinello-Rahman tau_p 2 ps) regarding reported parameters.[17,28] However, in some cases, this ensemble prevents the RNA system from producing reasonable unfolding results. As explained in detail below, when we checked the unfolding trajectory of the RNA system (WT-30nt system has been checked) with a 4–21.8 THz wave, we found that the water box would start to expand sharply at some moment. The water molecules would be unevenly distributed in the expanded region, with the average temperature rising by up to 21 K (set at 295 K), which is unreasonable. Nevertheless, the unfolding process of WT-30nt with the action of THz waves (0.1-3 THz and 23.8-41.2 THz) other than 4-21.8 THz did not show a sharp expansion of the water box and an uneven distribution of water molecules. Instead, the water box was almost unchanged, the water molecules were distributed evenly, the overall temperature increased to different degrees (the average temperature rose by 16 K), and the pressure was higher than the preset 1 bar to various degrees.

To solve the above problems of uneven distribution of water molecules and expansion of the water box, we successively adjusted tau_t (0.2 ps) to the limit time step of 2 fs, followed by replacing the Parrinello-Rahman pressure coupling for Berendsen and then changed the pressure coupling tau_p (2 ps) of Parrinello-Rahman to the minimum value of 0.8 ps. The above attempts alleviated the unfolding phenomenon of the time constant tau_t 0.2 ps but did not substantially change it. After a thorough investigation, we ended up with an NVT ensemble for the SMD simulation, controlling only the temperature (V-rescale tau_t 2 fs) and fixing the size of the water box.[51] Later, we set the pull type as Umbrella, set the pull direction in the y-axis, set the force constant as 1000 kJ/mol/nm^2, set two pull groups (one fix and pulling another), set the pull rate as 10 nm/ns (selected by testing different pulling rate), wrote out the pull force for each step, constrained all covalent bonds, and then pulled the system for 2.5 ns (or 5 ns) to fully unfolded RNAs. The simulations were repeated 20 times at each THz frequency condition. In Table S5, we presented the average temperature during the mechanical unfolding of RNA hairpins.

MD simulations of folded WT-30nt RNA

The amber14sb OL15 force field plus χOL3 RNA patch was also employed for MD simulation. We chose rigid TIP3P water and constrained bonds involving hydrogen atoms in pre-equilibrium. Then, we also used the V-rescale temperature coupling (303 K) and Berendsen pressure coupling (1 bar). In production MD, we adopted the Parrinello-Rahman pressure coupling while other settings remained the same. After that, we set the polarization direction of THz waves as Y (to keep consistent with the polarization direction of THz wave in WT-30nt SMD simulation) and picked up the frequencies of THz waves from the IR absorption spectrum of the folded WT-30nt. Each frequency was run for 30 ns (after 50 ns MD simulation) and 30 times, a time scale long enough to study the effects of THz waves on folded WT-30nt.

QUANTIFICATION AND STATISTICAL ANALYSIS

In this study, a comprehensive analysis of both the binding energy of MD-simulated RNA (Tables 1 and S1) and the energy involved in the SMD-simulated RNA unfolding process (Tables 2, S2, and S4) was conducted using a two-sided t-value test. A detailed explanation of each parameter of the t-value test can also be found in the corresponding table of the main text and supplemental information. The formula is as follows:

$$t = \frac{\mu_{noE} - \mu_{THz}}{\sqrt{\frac{\sigma_{noE}^2}{n} + \frac{\sigma_{THz}^2}{n}}} \quad \text{(Equation 3)}$$

μ_{noE}, μ_{THz}, σ, and n are the mean without THz waves, the mean with THz waves, the standard deviation (SD), and the sample value, respectively. For MD simulation, n=30, σ is the SD, $t_{0.1}(60)=1.671$. For SMD simulation, n=20, σ is the SD, $t_{0.05}(38)=2.024$, $t_{0.01}(38)=2.712$, and $t_{0.001}(38)=3.566$.